coatings

MDPI

Article

Bimetallic 3D Nickel-Manganese/Titanium Bifunctional Electrocatalysts for Efficient Hydrogen and Oxygen Evolution Reaction in Alkaline and Acidic Media

Sukomol Barua, Aldona Balčiūnaitė *, Jūrate Vaičiūnienė, Loreta Tamašauskaitė-Tamašiūnaitė and Eugenijus Norkus

Department of Catalysis, Center for Physical Sciences and Technology (FTMC), LT-10257 Vilnius, Lithuania; sukomol.barua@ftmc.lt (S.B.); jurate.vaiciuniene@ftmc.lt (J.V.); loreta.tamasauskaite@ftmc.lt (L.T.-T.); eugenijus.norkus@ftmc.lt (E.N.)

* Correspondence: aldona.balciunaite@ftmc.lt

Abstract: In this work, 3D nickel-manganese (NiMn) bimetallic coatings have been studied as electrocatalysts for both hydrogen evolution reaction (HER) and oxygen evolution reaction (OER) in alkaline (1.0 M KOH) media and the HER in acidic (0.5 M H_2SO_4) media. The catalysts have been deposited on a titanium substrate (1 × 1 cm^2) using low-cost and facile electrochemical deposition method through a dynamic hydrogen bubble template technique. The electrocatalytic performance of these fabricated catalysts was investigated by using Linear Sweep Voltammetry (LSV) for HER and OER at different temperatures ranging from 25 up to 75 °C and also was characterized by scanning electron microscopy (SEM) and inductively coupled plasma optical emission spectroscopy (ICP-OES). It was found that fabricated NiMn/Ti-5 electrocatalyst with Ni^{2+}/Mn^{2+} molar ratio of 1:5 exhibits excellent HER activity in alkaline media with overpotential of 127.1 mV to reach current density of 10 mA cm^{-2}. On the contrary, NiMn/Ti-1 electrocatalyst that fabricated with Ni^{2+}/Mn^{2+} molar proportion of 1:1 and lowest Mn-loading of 13.43 μgcm^{-2} demonstrates exceptional OER activity with minimum overpotential of 356.3 mV to reach current density of 10 mA cm^{-2}. The current densities increase ca. 1.8–2.2 times with an increase in temperature from 25 °C to 75 °C for both HER and OER investigation. Both catalysts also have exhibited excellent long-term stability for 10 h at constant potentials as well as constant current density of 10 mA cm^{-2} that assure their robustness and higher durability regarding alkaline water splitting.

Keywords: nickel; manganese; bifunctional electrocatalyst; electrodeposition; hydrogen evolution reaction; oxygen evolution reaction

Citation: Barua, S.; Balčiūnaitė, A.; Vaičiūnienė, J.; Tamašauskaitė-Tamašiūnaitė, L.; Norkus, E. Bimetallic 3D Nickel-Manganese/Titanium Bifunctional Electrocatalysts for Efficient Hydrogen and Oxygen Evolution Reaction in Alkaline and Acidic Media. *Coatings* **2023**, *13*, 1102. https://doi.org/10.3390/coatings13061102

Academic Editor: Rosalba Passalacqua

Received: 15 May 2023
Revised: 9 June 2023
Accepted: 13 June 2023
Published: 15 June 2023

1. Introduction

Over the last decade, a substantial research focusing on uninterrupted supply of renewable and clean energy has become a key issue due to alarming environmental threat and rapid depletion of fossil fuels [1–4]. In order to find potential substitutes, hydrogen is considered the most promising alternative to fossil fuels because of its advantages of zero carbon emissions, high gravimetric energy density (140 MJ·Kg^{-1}), and high efficiency [5–10]. Comparing with major methods for industrial hydrogen production e.g., coal gasification and steam methane reforming, the electrocatalytic water splitting in large-scale can also be considered as the most prospecting method [11]. This is not only due to the low conversion efficiency of methane and coal steam into H_2 and CO_2, and their consequences of carbon-emissions and global climate warming but also the advantageous feature of high purity industrial-level H_2 production from abundant natural resource with free-carbon emission and sustainability. This promising method of green H_2 production can also be the most convenient way to store the intermittent renewable energy like solar and wind energy by converting the electricity into H_2 fuels [12].

Electrocatalytic water splitting is regarded as a propitious approach for hydrogen production that consists of two half reactions: the anodic oxygen evolution reaction (OER) and the cathodic hydrogen evolution reaction (HER). The overall electrocatalytic water splitting under standard condition is a thermodynamically unfavorable uphill reaction that requires a thermodynamic Gibbs free energy of 237.2 kJ mol^{-1}, corresponding to the theoretical limit of 1.23 V. However, to drive the reaction at a practical rate, total energy of 285.8 kJ mol^{-1} is required that when converted to potential becomes 1.48 V, which is called the overpotential. Thus, practical real-world water spitting processes are limited by the high overpotential and can only be occurred by exceeding this barrier [13]. Nevertheless, two half-cell reactions of water splitting, i.e., HER and OER require large amount of energy to initiate and high individual overpotential to overcome sluggish multi-electron transfer kinetics, which leads to energy waste [14,15]. To overcome lethargic kinetics and for reducing high overpotential values of complex electron transfer pathways, currently, Pt-group and Pt-based materials (e.g., Pt/C) are considered as benchmark catalysts for HER and Ir/Ru-based (IrO_2/RuO_2) materials are considered the highly efficient commercially available catalysts for OER [16–19]. However, their low natural reserves and high cost restrict the large-scale industrial application of these catalysts and hinder the production and commercialization of hydrogen by electrocatalytic water spitting. Therefore, the designing and development of a cost-efficient, stable and highly efficient bifunctional electrocatalyst is the key factor to breaking the technical bottleneck of renewable green hydrogen production from overall water splitting [20,21].

In electrocatalytic water splitting, the mechanism of cathodic HER involves three main steps, i.e., Volmer, Heyrovsky and Tafel reactions, as shown below, in alkaline media, where the asterisk (*) represents the active sites on the surface of the electrocatalyst [22]:

$$\text{Volmer reaction: } H_2O + e^- + * \leftrightarrow H^* + OH^- \text{ (b} \sim 120 \text{ mV dec}^{-1}\text{)} \quad (1)$$

$$\text{Heyrovsky reaction: } H^* + H_2O + e^- \leftrightarrow H_2 + OH^- + * \text{ (b} \sim 40 \text{ mV dec}^{-1}\text{)} \quad (2)$$

$$\text{Tafel reaction: } H^* + H^* \leftrightarrow H_2 + 2^* \text{ (b} \sim 30 \text{ mV dec}^{-1}\text{)} \quad (3)$$

where b is the Tafel slope obtained from the HER polarization curves.

On the other hand, in alkaline electrolytes, the anodic OER mechanism involves the breaking of the O—H bond and the formation of the O—O bond and progresses through four electron transfer steps. The mechanism of OER has been shown in Equations (4)–(8) for alkaline medium [23].

$$OH^- + * \rightarrow OH^* + e^- \quad (4)$$

$$OH^* + OH^- \rightarrow O^* + H_2O + e^- \quad (5)$$

$$2O^* \rightarrow 2^* + O_2(g) \quad (6)$$

$$O^* + OH^- \rightarrow OOH^* + e^- \quad (7)$$

$$OOH^* + OH^- \rightarrow * + O_2(g) + H_2O(l) + e^- \quad (8)$$

In a quest to get over these energy consuming slothful multi-electron transfer kinetics and to promote potential substitutes of high-cost, noble metal-based electrocatalysts, an intense research interest has been paid on various transition metals based materials for exploring high-active electrocatalysts substantiating their cost, stability, efficiency and earth-abundance. In recent years, many non-noble transition metal-based compounds (especially 3*d*-block transition metals such as Ni, Co, Fe, Mo, Mn etc.) and their alloys [24–28], ox-

ides [29–32], hydroxides/layered double hydroxide (LDH) [33–36], oxyhydroxides [37–39], phosphides [40–44], sulfides [45–48] etc. have been explored and demonstrated excellent individual HER or OER performance as well as unique superior bifunctional electrocatalytic activity.

Among these electrocatalysts, nickel-based materials especially nickel-based bi- or, trimetallic and multicomponent alloy electrocatalysts can be considered as potential substitutes for noble metal catalysts due to their abundant reserves, low cost, unique electronic interaction, diversity of modification by optimizing the electronic structure, high electrical conductivity, excellent corrosion resistance, optimal stability, and excellent performance for the production of hydrogen in alkaline media [49–53]. In addition, nickel doping or alloying with other non-precious metals improve the electronic structure of the electrodes and proven as one of the most promising strategies for enhancement of electrocatalytic activity. For example, the addition of iron to the Ni–Mo electrodeposition bath leads to a synergistic effect on the deposition of molybdenum and the amount of molybdenum on the electrode surface increased from 9.3 to 37.4 atomic percent. The as-fabricated ($Ni_{52.3}Mo_{37.4}Fe_{10.2}$) electrocatalyst with optimal composition exhibits a small overpotential of 65 mV and 344 mV for delivering current density of 10 mA cm^{-2} on HER and OER, respectively in alkaline media [54]. An enhanced HER and OER activity have been demonstrated by Cu-doped Ni bifunctional electrocatalysts as require minimum overpotential of 76 mV and 290 mV, respectively to the current density of 10 mA cm^{-2} [55]. Gao et al. reported a ternary Ni-Fe-Mo alloy nanowire electrocatalyst ($Ni_{0.8}Fe_{0.15}Mo_{0.05}$) which exhibits prominently improved OER catalytic performance achieving an optimal overpotential of 300 mV at 50 mA cm^{-2} with corresponding Tafel slope value of 42.4 mV dec^{-1} [56]. All of these studies have shown that metal alloying prompts to improve electrocatalytic activity. In addition, Mn as one of the first-row transition metal element has received tremendous attention as dopant to decorate high-performance alloy electrocatalysts for overall water splitting [57]. Luo et al. synthesized Mn–Fe bimetallic oxide heterostructures on nickel foam by adjusting the molar ratio of Fe:Mn [58]. The MnFeO-NF-0.4 electrocatalyst with Fe:Mn ratio of 0.4:1 exhibited outstanding performance with ultralow overpotential of 157 mV for the OER while the MnFeO-NF-0.8 (Fe:Mn ratio of 0.8:1) demonstrated superior HER performance with only 64 mV overpotential to achieve a current density of 10 mA cm^{-2}. Xu et al. designed Mn-doped Ni_2P microflowers with optimal Mn/Ni ratio of 0.053 which outperforms many commercially used electrocatalysts exhibiting low overpotentials of 205 mV for HER and 330 mV for OER to achieve a current density of 100 mA cm^{-2} [59].

Moreover, another favorable approach to improve the electrocatalytic performance of catalysts is to increase the active surface area by creating a three-dimensional structure. Electrocatalyst in the form of three-dimensional coating is more suitable for practical application in comparison with powder as polymer binders are used to adhere powder electrocatalysts to the conducting surface, whereas, the catalyst on self-supporting electrodes are easy to operate and remain in direct contact with electrolytes, which can increase the conductivity and accelerate electron transfer. Additionally, the 3D interconnected network structure of the self-supporting electrode substrate is more favorable for the release of hydrogen and oxygen [60–62]. Answering above phenomena, the electrochemical deposition method is the facile, cost-effective, binder-free, template-free, versatile method to fabricate highly active electrocatalysts with desired composition and morphology.

To our knowledge, a number of NiMn LDH-based catalysts [34,63–69], their phosphides [70], phosphates [71], selenides [72] and composites [73] have been reviewed and investigated with different composition, morphology and fabrication conditions but only few works carried out on nickel-manganese bi- or, trimetallic alloy catalysts for electrocatalytic water splitting.

In this study, we report an affordable and facile fabrication of bimetallic NiMn alloy electrocatalysts demonstrating their superior bifunctional electrocatalytic performance for hydrogen evolution reaction in both alkaline and acidic media (1 M KOH and 0.5 M H_2SO_4) and the oxygen evolution reaction in alkaline media with excellent long-term stability.

2. Materials and Methods

2.1. Chemicals

Titanium foil (99.7% purity) and stainless steel foil (0.2 mm, Type 304) were purchased from Sigma-Aldrich (Saint Louis, MO, USA) Supply and Alfa Aesar (Karlsruhe, Germany) GmbH & Co., respectively. H_2SO_4 (96%), HCl (35–38%), nickel sulfate hexahydrate ($NiSO_4 \cdot 6H_2O$, >98%), manganese chloride tetrahydrate ($MnCl_2 \cdot 4H_2O$, >99%), ammonium sulfate ($(NH_4)_2SO_4$, >99%), boric acid (H_3BO_3, >99.5%) and KOH (98.8%) were purchased from Chempur Company (Karlsruhe, Germany). Ultrapure water with a resistivity of 18.2 MΩ cm^{-1} was used for preparing the solutions. All chemicals were of analytical grade and used directly without further purification.

2.2. Fabrication of Catalysts

In this study, titanium sheets were used as substrates to fabricate the bimetallic nickel-manganese alloy electrocatalysts with different compositions. The catalysts were prepared by a facile, low-cost electrochemical deposition method on Ti surface (1 × 1 cm^2) through a dynamic hydrogen bubble template technique. Initially, the titanium sheets were pretreated in diluted H_2SO_4 (1:1 vol.) at 70 °C for 3 s, then rinsed with distilled water and finally immersed into the electrochemical deposition bath. The composition of the coating bath for NiMn/Ti electrocatalysts included $NiSO_4 \cdot 6H_2O$ (52.57 g·L^{-1}), $MnCl_2 \cdot 4H_2O$ (39.60 to 197.92 g·L^{-1}), $(NH_4)_2SO_4$ (66.07 g·L^{-1}) and H_3BO_3 (18.55 g·L^{-1}) dissolved in distilled water at acidic condition (1.5 M H_2SO_4 and 1 M HCl). Also, 52.57 · g·L^{-1} of $NiSO_4$ $6H_2O$ and 197.92 g·L^{-1} of $MnCl_2 \cdot 4H_2O$ were used separately with aforementioned other reagents to prepare Ni/Ti and Mn/Ti catalyst samples, respectively, for comparing performances with fabricated catalysts. The composition of the electrochemical bath and electroplating conditions used for coating treatment are presented in Table 1. Electrochemical deposition was implemented in a two-electrode cell in which a stainless steel sheet (40 × 25 × 0.2 mm) was used as the anode. The fabrication procedure was carried out under the applied current density and duration time conditions of 50 mA cm^{-2} for 3 min and 500 mA cm^{-2} for another 3 min. After coating, the samples were taken out, thoroughly rinsed with deionized water, air-dried at room temperature and preserved for further investigations.

Table 1. The composition of the electrochemical bath with plating condition parameters.

Catalysts	Concentration (M)				Plating Conditions	
	$NiSO_4$ $6H_2O$	$MnCl_2$ $4H_2O$	$(NH_4)_2SO_4$	H_3BO_3	Parameters	Values
Ni/Ti	0.2	-	0.5	0.3	Current densities	50 mA cm^{-2}
Mn/Ti	-	1.0	0.5	0.3		500 mA cm^{-2}
NiMn/Ti-1	0.2	0.2	0.5	0.3	Time	3 min
NiMn/Ti-2	0.2	0.4	0.5	0.3		
NiMn/Ti-3	0.2	0.6	0.5	0.3	Temperature	25 °C
NiMn/Ti-4	0.2	0.8	0.5	0.3		
NiMn/Ti-5	0.2	1.0	0.5	0.3	pH	~1

2.3. Characterization of Catalysts

The morphology and composition of the prepared Ni/Ti sample and NiMn/Ti catalysts were investigated by scanning electron microscopy (SEM) using a SEM workstation SEM TM 4000 Plus (HITACHI) with an energy dispersive X-ray (EDX) spectrometer.

The metal loadings were determined by inductively coupled plasma optical emission spectroscopy (ICP–OES) analysis. The ICP–OES spectra were recorded using an Optima 7000DV spectrometer (Perkin Elmer, Waltham, MA, USA) at wavelengths of λ_{Ni} 231.604 nm and λ_{Mn} 257.610 nm.

2.4. Electrochemical Measurements

The electrocatalytic activity of bimetallic nickel-manganese electrocatalysts towards HER and OER was evaluated by linear sweep voltammetry (LSV) using a potentiostat PGSTAT302 (Metrohm Autolab B.V., Utrecht, The Netherlands) through Electrochemical Software (Nova 2.1.4). A standard three-electrode electrochemical cell was used during the investigation and the fabricated NiMn/Ti catalysts with a geometric area of 2 cm^2 were employed as working electrodes, a Pt sheet was used as a counter electrode and a saturated calomel electrode (SCE) was used as a reference. All potentials in this work were converted to the reversible hydrogen electrode (RHE) scale using the following equation:

$$E_{RHE} = E_{SCE} + 0.242\ V + 0.059\ V \times pH_{solution} \quad (9)$$

LSVs were recorded in an Ar-saturated 1 M KOH solution at the temperature range from 25 °C to 75 °C, setting the temperature with a water jacket connected to a LAUDA Alpha RA 8 thermostat. HER and OER polarization curves were recorded from the open circuit potential (OCP) to −0.432 V (vs. RHE) and OCP to 2.068 V (vs. RHE), respectively, at a potential scan rate of 10 mV s^{-1}. The HER polarization curves in acidic media (0.5 M H_2SO_4) were recorded from the OCP to −0.958 V (vs. RHE) at a potential scan rate of 10 mV s^{-1}. Also, in order to evaluate the long-term stability of the fabricated catalysts, the chronopotentiometric curves were recorded at a constant current density of 10 mA cm^{-2} in 1.0 M KOH solution for 10 h. Moreover, the chronoamperometry (CA) curves were also studied after 10 h continuous electrolysis in alkaline environment at a potential of −0.232 V (vs. RHE) for HER and at a potential of 1.818 V (vs. RHE) for OER.

3. Results and Discussions

3.1. Microstructure and Morphology Studies

In this study, the electrocatalytic performance of 3D bimetallic nickel-manganese alloy electrocatalysts were evaluated for HER and OER in the alkaline (1.0 M KOH) medium as well as the HER activity in acidic (0.5 M H_2SO_4) medium. The coatings' surface morphology was studied by scanning electron microscopy (SEM). Figure 1 depicted the SEM images of the prepared Ni/Ti (a) sample and NiMn/Ti-1 (b), NiMn/Ti-2 (c), NiMn/Ti-3 (d), NiMn/Ti-4 (e) NiMn/Ti-5 (f) catalysts. The surface morphology of Ni/Ti sample is observed to be compact, smooth and crack-free where the Ni particles are seem to be uniformly distributed. The top side views of NiMn/Ti catalysts demonstrate a typical globular morphology consisting of smaller nodules in Figure 1b. The size of nodules enlarged with increase of Mn-content on the catalyst and started to cover the surface of substrate (Figure 1c,d). With higher Mn-content, the catalysts turned into a unique porous architecture with abundant pores of different sizes, which can provide more channels for electrolyte diffusion, accelerate the efficiency of electron transport and increase numerous active sites (Figure 1e,f).

Mass of the elements (metal loadings) deposited onto the Ti substrate surface was determined by ICP–OES analysis (Table 2). It can be seen that the fabricated bimetallic NiMn/Ti electrocatalysts possessed ca. 44–86.6 wt% of Ni and ca. 13.4–56 wt.% of Mn. The total metal loadings ($\mu g_{metal} cm^{-2}$) in the prepared catalysts were gradually uplifted with increase of Mn-concentration and vary from ca. 100 up to 1223.5 $\mu g_{metal} cm^{-2}$.

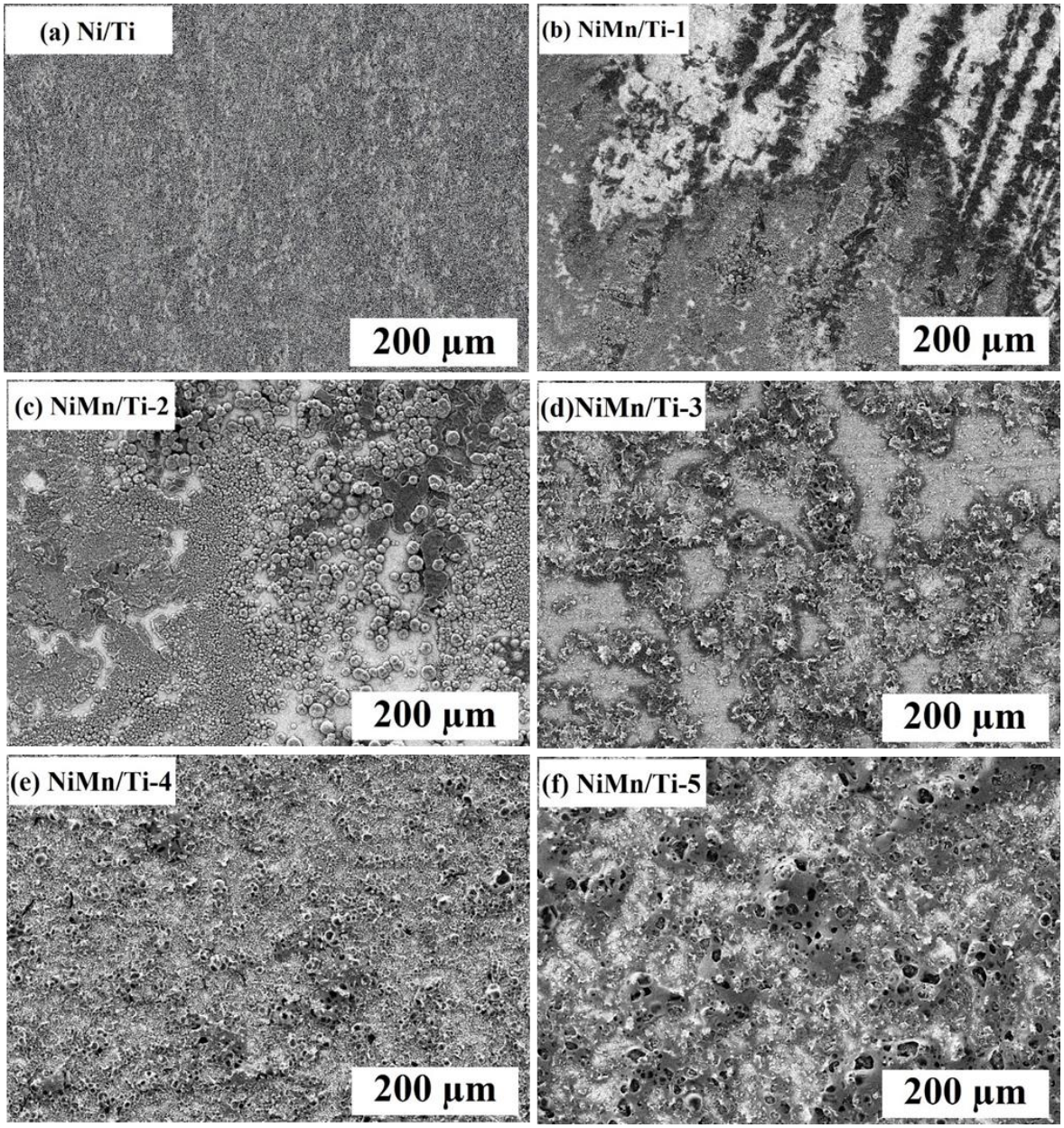

Figure 1. SEM views of Ni/Ti sample (**a**) and bimetallic NiMn/Ti catalysts (**b**–**f**).

Table 2. The metal loading in the catalysts as determined by ICP-OES analysis.

Catalyst	Ni Loading ($\mu g_{Ni} cm^{-2}$)	Mn Loading ($\mu g_{Mn} cm^{-2}$)	Total Metal Loading ($\mu g_{metal} cm^{-2}$)	Wt.%	
				Ni	Mn
Mn/Ti	-	21.5	21.5	-	100
Ni/Ti	300.25	-	300.25	100	-
NiMn/Ti-1	86.55	13.43	99.98	86.56	13.44
NiMn/Ti-2	126.4	40.55	166.95	75.71	24.29
NiMn/Ti-3	269.7	105.25	374.95	71.93	28.07
NiMn/Ti-4	448.45	374.4	822.85	54.49	45.51
NiMn/Ti-5	538	685.5	1223.5	43.97	56.03

3.2. Electrocatalytic Activity towards HER

The electrocatalytic performance of the prepared catalysts for HER was investigated by recording LSVs in 1.0 M KOH solution at a potential scan rate of 10 mV·s^{-1} from OCP up to −0.432 V (vs. RHE), at temperature from 25 up to 75 °C. The current density increases ca. 1.85–2.25 times with an increase in temperature from 25 up to 75 °C using the fabricated 3D NiMn/Ti catalysts for HER. The LSV curves are shown in Figure 2 at the range of investigated temperatures and the polarization curves of fabricated catalysts at only 25 °C are discretely demonstrated in Figure 3a with prepared bare Ni/Ti and Mn/Ti catalysts from Ni and Mn-solution.

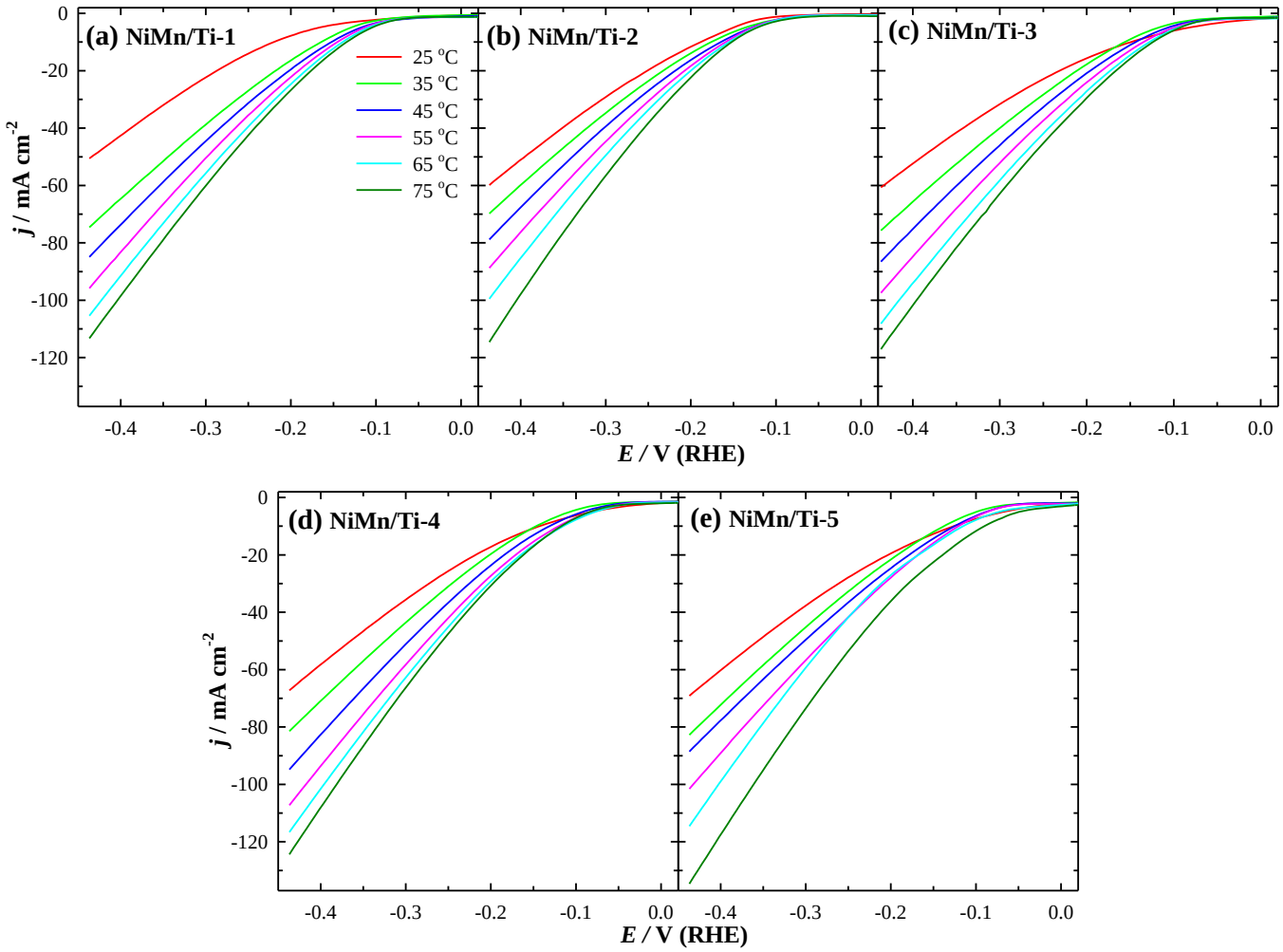

Figure 2. HER polarization curves of 3D NiMn/Ti catalysts in 1 M KOH solution at 10 mV s^{-1} potential scan rate and a temperature range from 25 up to 75 °C.

As shown in Figure 3a, all fabricated NiMn/Ti catalysts exhibit remarkable HER catalytic activities surpassing those of Ni/Ti and Mn/Ti samples. It is worth mentioning that via alloying Ni to Mn with different molar ratio enhanced the electrocatalytic activity and the overpotential values at 10 mA cm^{-2} (η_{10}) were considerably reduced from 424.2 mV for Mn/Ti sample to 220.3 mV for NiMn/Ti-1 catalyst. The bimetallic NiMn/Ti-5 delivers superior catalytic activity with a low overpotential of 127.1 mV to achieve 10 mA cm^{-2} relative to the NiMn/Ti-4 (144.8 mV) and NiMn/Ti-3 (149.8 mV) catalysts (Table 3). The obtained results show that the overpotential for HER in alkaline media is shifted to a more positive potential region with the increase of Mn in the coatings.

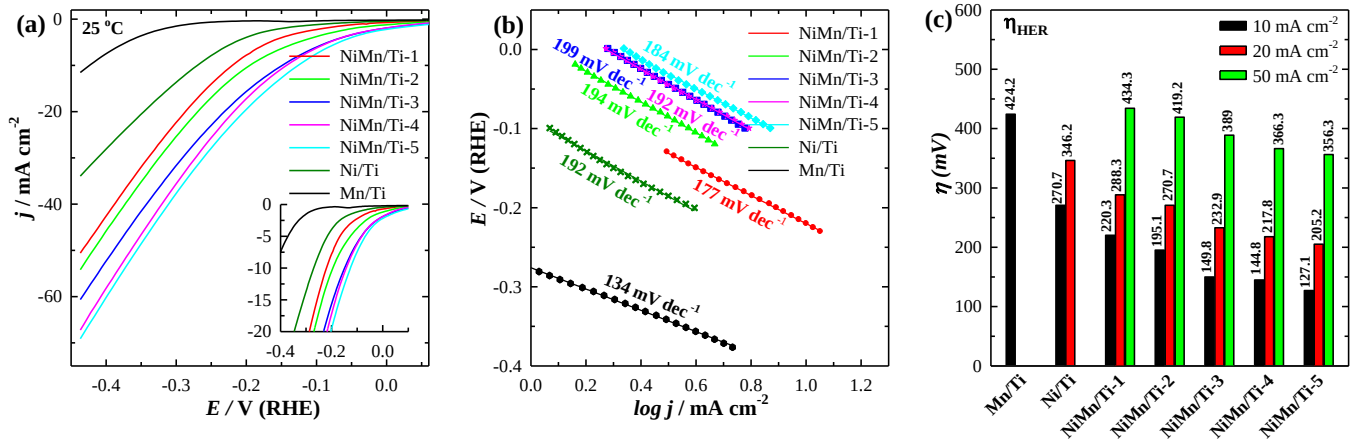

Figure 3. HER polarization curves in 1 M KOH solution at 10 mV s^{-1} potential scan rate and at 25 °C temperature (**a**) with corresponding extracted Tafel plots (**b**) and required overpotentials to reaching the current densities of 10, 20 and 50 mA cm^{-2} (**c**).

Table 3. Electrochemical parameters of the investigated catalysts toward HER in alkaline media.

Catalysts	*j* (mA cm^{-2}) in Different Temperatures (°C) at −0.432 V(vs. RHE)						*j* (mA μg^{-1}) at 25 °C	η_{10} (mV) at 25 °C	Tafel Slope (mV dec^{-1})
	25	35	45	55	65	75			
Mn/Ti	11.53	-	-	-	-	-	0.54	424.2	134
Ni/Ti	33.95	-	-	-	-	-	0.11	270.7	192
NiMn/Ti-1	50.58	74.57	84.92	95.81	105.39	113.28	0.51	220.3	177
NiMn/Ti-2	59.85	69.79	78.84	88.75	99.49	114.56	0.36	195.1	194
NiMn/Ti-3	60.65	75.68	86.56	97.46	108.15	117.03	0.16	149.8	199
NiMn/Ti-4	67.25	81.47	94.82	107.25	116.65	124.41	0.08	144.8	192
NiMn/Ti-5	69.12	82.75	88.56	101.6	114.59	134.67	0.06	127.1	184

To reveal the HER kinetics behavior, the NiMn/Ti electrocatalysts were investigated using Tafel plots. The Tafel equation (Equation (10)) was used for the determination of the kinetic parameters for the HER:

$$\eta = a + b\log j \quad (10)$$

where, η (V), a (V), b (V dec^{-1}) and *j* (A cm^{-2}) represent the applied overpotential, the curve intercept, the Tafel slope and the resulting current density, respectively. Tafel slope values were found to be 177, 194, 199, 192, and 184 mV dec^{-1} (Figure 3b and Table 3) for the prepared 3D bimetallic NiMn/Ti-1, NiMn/Ti-2, NiMn/Ti-3, NiMn/Ti-4, and NiMn/Ti-5 catalysts, respectively, implying that HER might occur through the Volmer–Heyrovsky mechanism. To evaluate the electrocatalytic activity of catalysts, it is important to compare the required overpotential to reach a current density of 10 mA cm^{-2} (η_{10}) that considered a benchmark in many studies. The magnitude of overpotentials required to reach current densities of 10, 20 and 50 mA cm^{-2} were shown in Figure 3c. It has been seen that alloying Ni to Mn with higher concentrations prompt to enhance the electrocatalytic activity and lowering overpotentials for HER, thus, the η_{10}, η_{20} and η_{50} values have followed a sequential downward order from NiMn/Ti-1 to NiMn/Ti-5.

Subsequently, the electrocatalytic activities of the prepared 3D NiMn/Ti catalysts for HER were also investigated in acidic media (0.5 M H_2SO_4) at a potential scan rate of 10 mV s^{-1} from OCP up to −0.958 V (vs. RHE). As evident from LSVs shown in Figure 4a, all studied catalysts exhibited excellent HER performance at 25 °C in comparison with prepared samples, while an optimal HER catalytic activity was observed on NiMn/Ti-5

with minimum overpotential of 102.1 mV to reach current density of 10 mA cm^{-2}, followed by NiMn/Ti-4 (160.1 mV) and NiMn/Ti-3 (177.7 mV).

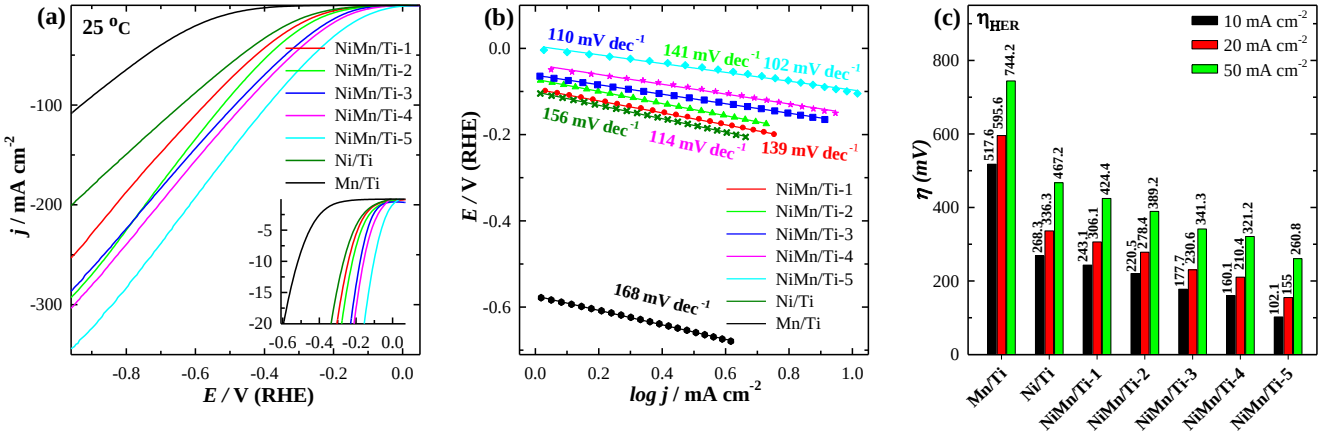

Figure 4. HER polarization curves of 3D NiMn/Ti catalysts in 0.5 M H_2SO_4 solution at a potential scan rate of 10 mV s^{-1} and 25 °C temperature (**a**). with corresponding extracted Tafel plots (**b**) and required overpotentials to reaching the current densities of 10, 20 and 50 mA cm^{-2} (**c**).

The polarization curves were then used for constructing the Tafel plots and calculating the Tafel slopes. The lowest Tafel slope value of 102 mV dec^{-1} was found for NiMn/Ti-5 electrocatalyst. Higher values of 114, 110, 141, and 139 mV dec^{-1} were determined at NiMn/Ti-4, NiMn/Ti-3, NiMn/Ti-2 and NiMn/Ti-1, respectively (Figure 4b and Table 4). The overpotentials required to reach current density of 10 mA cm^{-2} for all catalysts were shown in Figure 4c and Table 4 and all values followed the similar lowering order likewise as alkaline media from NiMn/Ti-1 to NiMn/Ti-5 catalysts.

Table 4. Electrochemical parameters of the investigated catalysts toward HER in acidic media.

Catalysts	*j* (mA cm^{-2}) at 25 °C	*j* (mA μg^{-1}) at 25 °C	η_{10} (mV) at 25 °C	Tafel Slope (mV dec^{-1})
Mn/Ti	108.67	5.05	517.6	168
Ni/Ti	201.13	0.67	268.3	156
NiMn/Ti-1	253.59	2.54	243.1	139
NiMn/Ti-2	293.17	1.76	220.5	141
NiMn/Ti-3	286.79	0.77	177.7	110
NiMn/Ti-4	303.79	0.37	160.1	114
NiMn/Ti-5	344.59	0.28	102.1	102

3.3. Electrocatalytic Activity towards OER

The electrocatalytic OER performance of fabricated 3D bimetallic NiMn/Ti catalysts was also thoroughly investigated in the alkaline (1.0 M KOH) electrolyte. The polarization curves were recorded in 1.0 M KOH solution at a potential scan rate of 10 mV·s^{-1} from OCP up to 2.068 V (vs. RHE) in the temperature range of 25–75 °C (Figure 5). The current densities increased ca. 1.77–2.21 times within this investigated range of temperature and it was observed that NiMn/Ti-1 exhibits much higher OER activity, needing a low overpotential of 356.3 mV at 10 mA cm^{-2} as compared to the NiMn/Ti-2 (361.4 mV) and NiMn/Ti-3 (371.4 mV) catalysts.

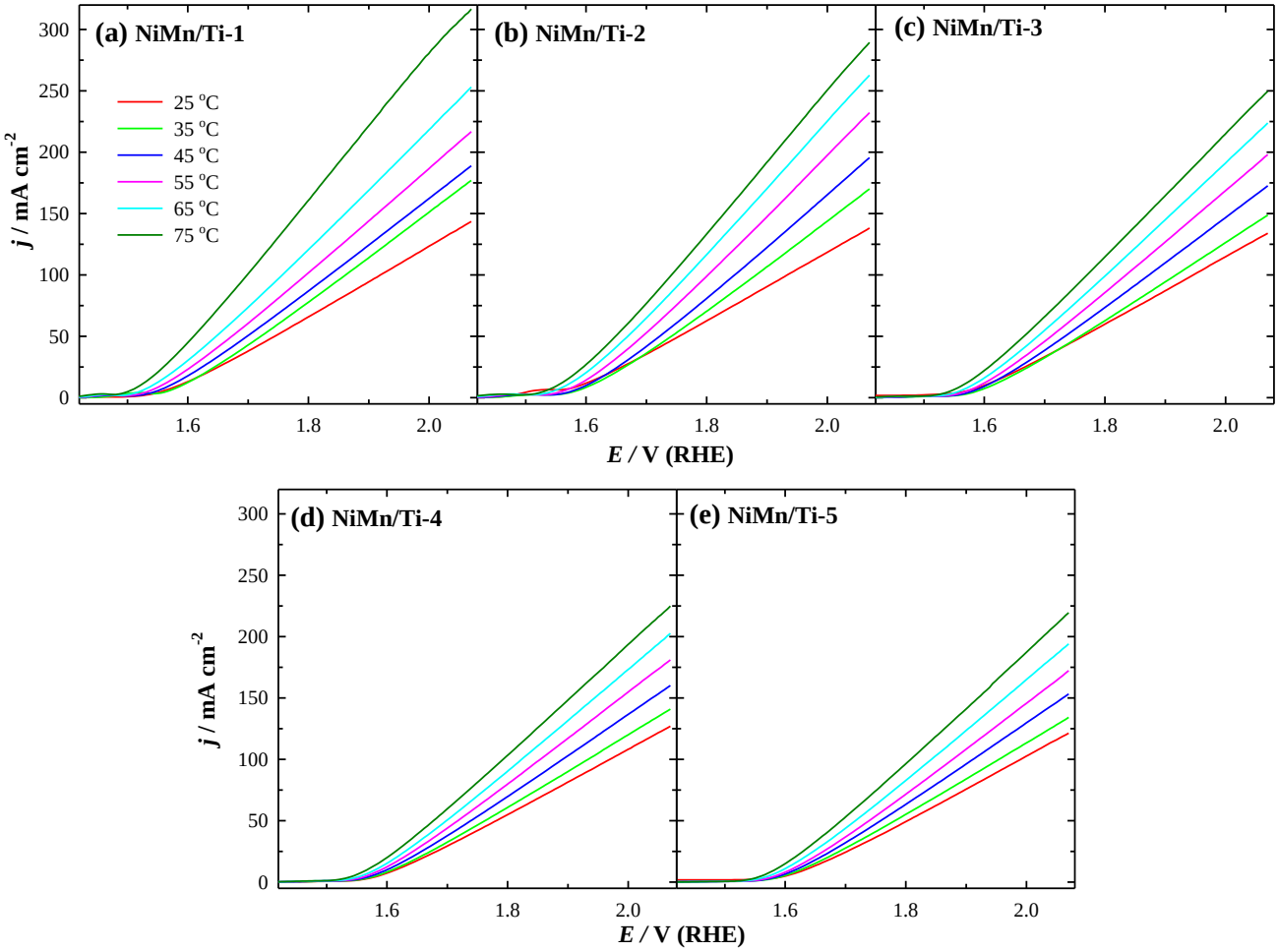

Figure 5. OER polarization curves of 3D NiMn/Ti catalysts in 1 M KOH solution at 10 mV s^{-1} potential scan rate and a temperature range from 25 up to 75 °C.

Figure 6a demonstrates the OER activity of all fabricated catalysts at 25 °C and it was observed that the catalysts prepared via alloying Ni to Mn with different proportion ratios notably prompt to enhance their electrocatalytic activity. The achieved overpotentials value at 10 mA cm^{-2} (η_{10}) of the prepared NiMn/Ti catalysts were remarkably reduced from Ni/Ti (449.5 mV) and Mn/Ti (671.1 mV) samples.

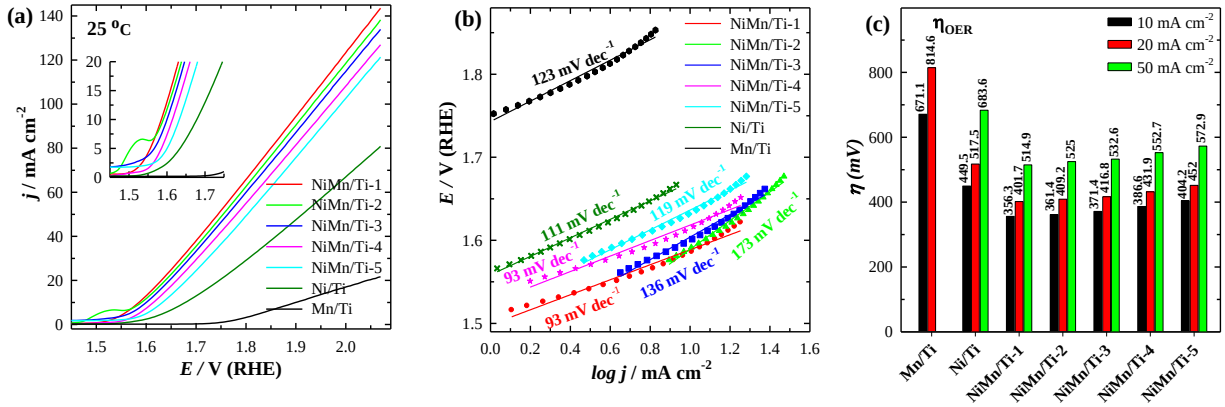

Figure 6. OER polarization curves at 25 °C temperature (**a**) with corresponding extracted Tafel plots (**b**) and required overpotentials to reaching the current densities of 10, 20 and 50 mA cm^{-2} (**c**).

The OER LSVs at 25 °C were then further used for constructing the Tafel plots and calculating the Tafel slopes. The Tafel slope for NiMn/Ti-1 was 93 mV dec^{-1}, which is lower than NiMn/Ti-2 (173 mV dec^{-1}), NiMn/Ti-3 (136 mV dec^{-1}) and NiMn/Ti-5 (119 mV dec^{-1}) (Figure 6b and Table 5).

Table 5. Electrochemical parameters of the investigated catalysts toward OER in alkaline media.

Catalysts	*j* (mA cm^{-2}) in Different Temperatures (°C) at 2.068 V						*j* (mA μg^{-1}) at 25 °C	η_{10} (mV) at 25 °C	Tafel Slope (mV·dec^{-1})
	25	35	45	55	65	75			
Mn/Ti	21.64	-	-	-	-	-	1.0	671.1	123
Ni/Ti	80.89	-	-	-	-	-	0.27	449.5	111
NiMn/Ti-1	143.54	177.03	188.96	216.81	253.04	316.7	1.44	356.3	93
NiMn/Ti-2	138.28	170.03	195.53	232.16	262.74	289.38	0.83	361.4	173
NiMn/Ti-3	133.94	148.77	172.7	198.04	223.88	249.68	0.36	371.4	136
NiMn/Ti-4	126.97	140.93	160.16	181.08	202.56	224.84	0.15	386.6	93
NiMn/Ti-5	121.35	134.16	153.26	172.24	194.09	219.53	0.1	404.2	119

Moreover, the overpotentials to reach current densities of 10, 20 and 50 mA cm^{-2} at 25 °C were also shown in Figure 6c and Table 5 and the η_{10}, η_{20} and η_{50} values have found to follow a sequential upward order from NiMn/Ti-1 to NiMn/Ti-5 catalysts. For instance, the η_{10}, η_{20} and η_{50} values were 356.3 mV, 401.7 mV and 514.9 mV for NiMn/Ti-1 as compared to 404.2 mV, 452 mV and 572.9 mV for NiMn/Ti-5, respectively, which certainly indicate the superior catalytic activity and favorable OER kinetics of NiMn/Ti-1 over the NiMn/Ti-5 electrocatalyst. A recent study also revealed that the OER performance of Ni_x | $Mn_{1-x}O$/CNTs electrocatalysts is significantly dependent on the content ratios of Ni and Mn. When the content of Mn element was more than 17%, the overpotential of catalyst increases, i.e., lowering Mn content notably improved the OER activity [74].

Furthermore, in order to compare the electrocatalytic activity of the prepared 3D bimetallic NiMn/Ti catalysts, the current density values were normalized in reference to the metals loadings for each catalyst to represent the mass activity of catalysts towards the HER and OER at 25 °C temperature (Tables 3–5). The highest mass electrocatalytic activity has been exhibited by NiMn/Ti-1 catalyst for HER in both acidic (2.54 mA μg^{-1}) and alkaline (0.51 mA μg^{-1}) media as well as for OER in alkaline (1.44 mA μg^{-1}) media with minimum metal loading of 99.98 $\mu g\ cm^{-2}$. It is worth mentioning that the mass activity of catalysts for both HER and OER has gradually declined with increase of Mn-loadings on prepared catalysts as higher Mn-concentration in coating bath favors the alloying of metals (Ni and Mn) via electrodeposition process and enriched the total metal loadings.

3.4. Electrocatalytic Stability Studies for HER and OER

To investigate the practical application and efficiency of any fabricated electrocatalysts, the desired electrocatalytic performance is not sufficient enough, and in addition, the electrocatalytic activity must be sustainable as long-term stability directly determines whether the materials can be developed for practical applications. Electrocatalytic stability is also directly related to the lifetime of the electrodes that regulates the production cost of hydrogen.

As the above mentioned investigations in alkaline and acidic media revealed that prepared bimetallic NiMn/Ti-5 electrocatalyst has excellent HER catalytic activity in both electrolytes and fabricated NiMn/Ti-1 electrocatalyst exhibits superior OER performance in alkaline media, thus in this section, the electrocatalytic stability of these two electrodes was investigated using different electrochemical methods. At first, the electrocatalytic durability was studied by Chronopotentiometry (CP) for 10 h. CP investigations were performed in 1.0 M KOH at a current density of 10 mA cm^{-2} at 25 °C (Figure 7).

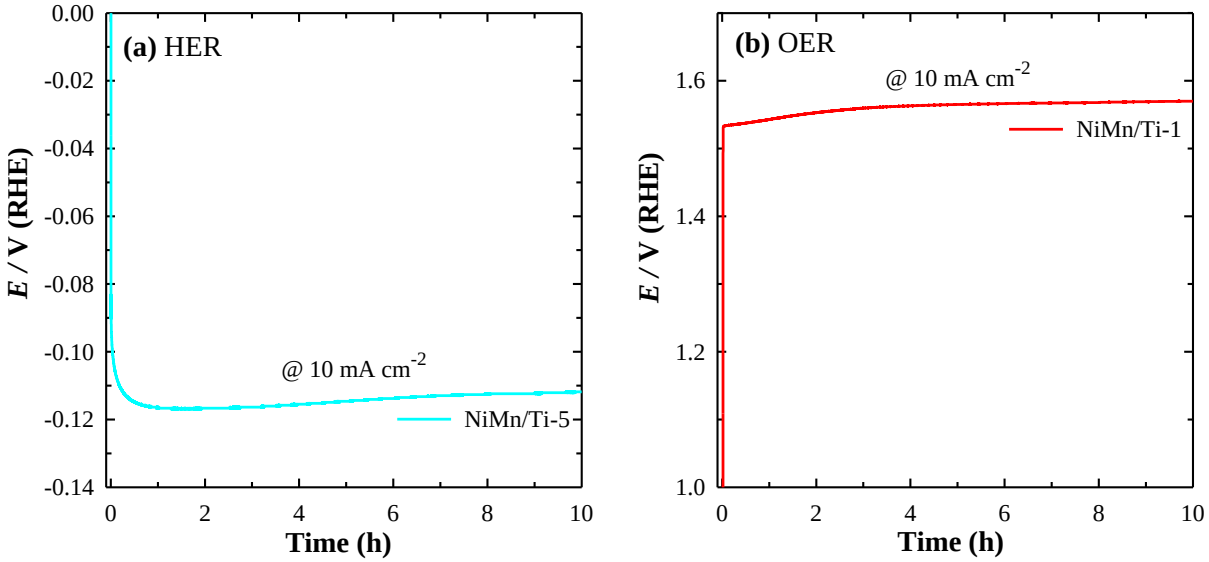

Figure 7. CP curves in 1.0 M KOH solution at a constant current density of 10 mA cm^{-2} at 25 °C of the investigated NiMn/Ti-5 for HER (**a**) and NiMn/Ti-1 for OER (**b**) electrocatalysts.

It was observed that the potential of ca. 115 mV of NiMn/Ti-5 as HER electrocatalyst (Figure 7a) and of ca. 335 mV of NiMn/Ti-1 as OER electrocatalyst (Figure 7b) was achieved at current density of 10 mA cm^{-2}. The CP curves did not deteriorate significantly after 10 h continuous HER and OER electrolysis at a static current density of 10 mA cm^{-2}, proving their good electrocatalytic stability for HER and OER in an alkaline environment.

Additionally, the electrocatalytic stability of these two catalysts has been examined by CA as well. CA investigations were carried out in 1.0 M KOH at −0.232 V (vs. RHE) and 1.818 V (vs. RHE) at 25 °C for the NiMn/Ti-5 and NiMn/Ti-1 electrocatalysts, respectively (Figure 8).

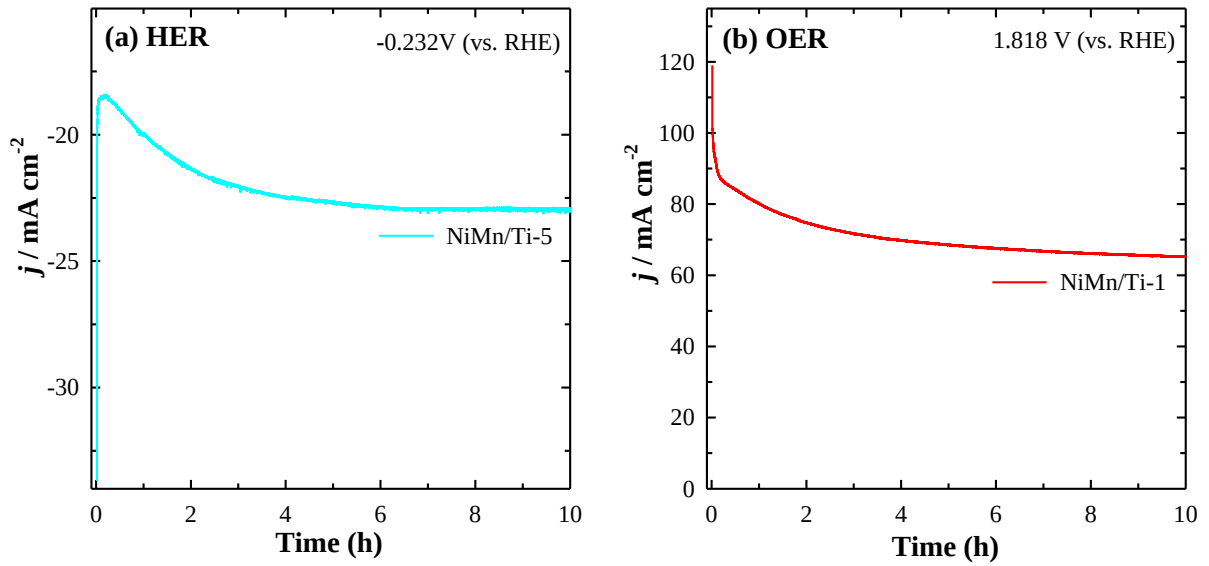

Figure 8. CA curves of the investigated NiMn/Ti-5 (**a**) and NiMn/Ti-1 (**b**) electrocatalysts in 1.0 M KOH solution at 25 °C at the potential values of −0.232V (vs. RHE) and 1.818 V (vs. RHE), respectively.

In this test, the electrocatalytic durability of both catalysts was studied by constant applied potential to the electrode and then the current density was monitored over time. After 10 h of investigation, approx. 6% degradation of current density was observed for NiMn/Ti-5 catalyst and the NiMn/Ti-1 catalyst has found to retain more than 92% of

its current, indicating their quite reasonable electrocatalytic stability in alkaline media as cathodic and anodic materials, respectively.

A comparison of HER and OER performance using herein-tested NiMn/Ti catalysts with some of the transition metal-based electrodes reported in the literature (Tables 6 and 7) demonstrates that these bimetallic catalysts exhibit comparable overpotentials and Tafel slopes for HER and OER.

Table 6. Electrochemical performance of herein tested catalysts towards HER in alkaline and acidic media with comparison of transition metal-based electrodes reported in the literatures.

Catalysts	Overpotential@Current Density (mV@mA cm^{-2})	Tafel Slope (mV dec^{-1})	Temperature (°C)	Electrolyte	Ref.
Ni-Mn/Cu Ni-Fe-Mn/Cu	101@10 64@10	118 68	-	1 M KOH	[28]
Ni-Fe/NF	142@10	133.3	-	1 M KOH	[52]
Ni_1Mn_1P Ni_2Mn_1P Ni_3Mn_1P	160@10 120@10 140@10	109 82 93	-	1 M KOH	[70]
Mn-doped Ni_2P Mn-doped Fe_2P Mn-doped Ni_2P/Fe_2P	160@10 136@10 90@10	124.27 142.34 115.41	-	1 M KOH	[75]
Mn-$Ni(OH)_2$ NiS_x Mn-NiS_x	197@10 172@10 94.2@10	134.5 111.9 71.5	-	1 M KOH	[76]
Ni-Fe/Cu	124@10	114	-	1 M KOH	[77]
$(Co,Fe)PO_4$	122@10	71	-	1 M KOH	[78]
$NiFe_{10}Se_{10}$@NF	154@10	129.3	-	1 M KOH	[79]
$FeSe_2$-$MoSe_2$(1-1)/rGO	178@10	80		1 M KOH	[80]
Ni–Mo/WC 3	134@10	163	25	1 M KOH	[81]
Ni-Co-Se@NiCo-LDH/NF Ni-Co-Fe-Se@NiCo-LDH/NF	189@10 113@10	124.09 44.87	-	1 M KOH	[82]
NC-1@CoO/NF NC-2@CoO/NF NC-3@CoO/NF NC-4@CoO/NF	241@10 139@10 192@10 196@10	155 96 189 141	-	1 M KOH	[83]
NiMo/FTO	154@10	152	25	1 M KOH	[84]
W_2C@CNT Mo_2C@CNT	125@10 118@10	104 92	-	1 M KOH	[85]
Ni-GF/VC Ni-GF/Fe_3C	128@10 93@10	80 63	-	1 M KOH	[86]
NiMn/Ti-1 NiMn/Ti-2 NiMn/Ti-3 NiMn/Ti-4 NiMn/Ti-5	220.3@10 195.1@10 149.8@10 144.8@10 127.1@10	177 194 199 192 184	25	1 M KOH	This work
NiMn/Ti-1 NiMn/Ti-2 NiMn/Ti-3 NiMn/Ti-4 NiMn/Ti-5	243.1@10 220.5@10 177.7@10 160.1@10 102.1@10	139 141 110 114 102	25	0.5 M H_2SO_4	This Work

Table 6. *Cont.*

Catalysts	Overpotential@Current Density (mV@mA cm^{-2})	Tafel Slope (mV dec^{-1})	Temperature (°C)	Electrolyte	Ref.
NiMo/FTO	140@20	118	25	0.5 M H_2SO_4	[84]
W_2C@CNT Mo_2C@CNT	155@10 121@10	85 77	-	0.5 M H_2SO_4	[85]
Ni-GF/VC Ni-GF/Fe_3C	111@10 112@10	86 97	-	0.5 M H_2SO_4	[86]
Mo_2C-RGO (3.0 wt %)	125@10	89	25	0.5 M H_2SO_4	[87]
Mo_2C P/Mo_2C F	118@10	48.6	-	0.5 M H_2SO_4	[88]
Ni-Pt nanofilm	90@10	49	25	0.5 M H_2SO_4	[89]
MoP FeS-MoP MnS-MoP	115@10 89@10 88@10	87 70 68	-	0.5 M H_2SO_4	[90]
Mo_2N-Mo_2C/NC	114@10	62	-	0.5 M H_2SO_4	[91]

NF—nickel foam, rGO—reduced graphene oxide, WC—tungsten carbide, CNT—carbon nanotube, LDH/NF—Layered double hydroxide/nickel foam, FTO—F-doped SnO_2, Ni-GF—Ni foam coated with graphene, F—microflower, NC—N-doped carbon framework.

Table 7. Electrochemical performance of herein tested catalysts towards OER in alkaline media with comparison of transition metal-based electrodes reported in the literatures.

Catalysts	Overpotential@Current Density (mV@mA cm^{-2})	Tafel Slope (mV dec^{-1})	Electrolyte	Ref.
$CoNi_2S_4$ (GCN)30/NF $CoNi_2S_4$ (GCN)50/NF $CoNi_2S_4$ (GCN)100/NF	340@30 310@30 350@30	93.21 49.86 109.01	1.0 M KOH	[48]
NMF-6 ($Ni_{52.3}Mo_{37.4}Fe_{10.2}$)	344@10	-	1.0 M KOH	[54]
Ni_1Mn_1 LDH Ni_3Mn_1 LDH Ni_5Mn_1 LDH	420@10 350@10 390@10	41 40 40	1.0 M KOH	[64]
NiMn LDH/$NiCo_2O_4$	310@10	99	1.0 M KOH	[67]
Ni-Mn LDH 21.1% Co-doped Ni-Mn LDH	385@10 310@10	80 59	1.0 M KOH	[68]
Ni_1Mn_1P Ni_2Mn_1P Ni_3Mn_1P	250@20 340@20 330@20	63 93 89	1.0 M KOH	[70]
$Ni_{0.95}$	$Mn_{0.05}O$/CNT $Ni_{0.83}$	$Mn_{0.17}O$/CNT	293@10 316@10	55.6 63.5	1.0 M KOH	[74]
NC-1@CoO/NF NC-2@CoO/NF NC-3@CoO/NF NC-4@CoO/NF	340@10 290@10 335@10 370@10	93 82 127 91	1.0 M KOH	[83]

Table 7. *Cont.*

Catalysts	Overpotential@Current Density (mV@mA cm^{-2})	Tafel Slope (mV dec^{-1})	Electrolyte	Ref.
$Ni_{1.5}Co_{1.5}P$/MF	314@10	71	1.0 M KOH	[92]
Ni_2Co_1P/MF	342@10	83		
Ni_1Co_2P/MF	387@10	114		
Ni_3S_2/NF	362@10	56.5	1.0 M KOH	[93]
Cu_2S-Ni_3S_2/NF	329@10	44.11		
MCS@a-Ni_3S_2	333@10	150.1	1.0 M KOH	[94]
Ni_3S_2@3-D GNs	305@10	50	1.0 M KOH	[95]
NiMn/Ti-1	356.3@10	93	1.0 M KOH at 25 °C	This work
NiMn/Ti-2	361.4@10	173		
NiMn/Ti-3	371.4@10	136		
NiMn/Ti-4	386.6@10	93		
NiMn/Ti-5	404.2@10	119		

GCN/NF—graphitic carbon nitride/nickel foam, LDH—layered double hydroxide, MF—microflower, MCS@a-Ni_3S_2—Mn-Cd-S@amorphous-Ni_3S_2, 3-D GNs—3-D graphene nanosheets, CNT—carbon nanotube.

4. Conclusions

In summary, a set of self-supported three-dimensional bimetallic NiMn alloy catalysts with various Ni:Mn molar ratios have been successfully synthesized through electrochemical deposition technique and their electrocatalytic activity for HER and OER was studied. The surface morphology demonstrates a unique 3D porous architecture that could avail numerous active sites and channels for electrolyte/gas diffusion. Electrochemical performance results manifested that the amalgamation of Mn element with Ni remarkably enhanced the electrocatalytic activity of the catalysts for HER and OER. The NiMn/Ti-5 electrocatalyst exhibited excellent HER activity with a low overpotential of 102.1 mV in acidic media and 127.1 mV in alkaline media to generate current densities of 10 mA cm^{-2}, respectively. On the contrary, NiMn/Ti-1 electrocatalyst with least Mn-content exhibits superior OER activity with a small overpotential of 356.3 mV to reach 10 mA cm^{-2}. Furthermore, the present electrocatalysts also demonstrated outstanding electrocatalytic long-term durability in an alkaline environment as the recorded potentials did not change significantly after 10 h continuous HER and OER electrolysis at a constant current density of 10 mA cm^{-2}.

This work tends to highlight the fabrication of Mn-containing bimetallic alloy catalysts as well as prioritize to increase the electrochemical active surface area of catalysts via 3D structure formation. The intrinsic activity of these 3D alloy catalysts will provide a strong guide for manufacturing bifunctional electrocatalysts for water splitting application with excellent comprehensive performance and the synergistic effects between transition elements may surpass the heteroatom doping strategy for enhancing the electrocatalytic performance.

Author Contributions: Conceptualization, A.B. and E.N.; methodology, S.B. and J.V; formal analysis, S.B.; investigation, S.B. and. J.V.; data curation, L.T.-T.; writing—original draft preparation, S.B. and A.B; writing—review and editing, E.N. and A.B.; visualization, L.T.-T.; supervision, A.B. All authors have read and agreed to the published version of the manuscript.

Funding: This research received no external funding.

Institutional Review Board Statement: Not applicable.

Informed Consent Statement: Not applicable.

Data Availability Statement: The data presented in this study are available on request from the corresponding author.

Conflicts of Interest: The authors declare no conflict of interest.

References

1. Zhou, Z.; Pei, Z.; Wei, L.; Zhao, S.; Jian, X.; Chen, Y. Electrocatalytic hydrogen evolution under neutral pH conditions: Current understandings, recent advances, and future prospects. *Energy Environ. Sci.* **2020**, *13*, 3185–3206. [CrossRef]
2. Zhu, L.; Li, C.; Li, H.; Li, H.; Wu, Z.; Huang, Y.; Zhu, X.; Sun, Y. Adjustable antiperovskite cobalt-based nitrides as efficient electrocatalysts for overall water splitting. *J. Mater. Chem. A* **2022**, *10*, 15520–15527. [CrossRef]
3. Ali, A.; Long, F.; Shen, P.K. Innovative strategies for overall water splitting using nanostructured transition metal electrocatalysts. *Electrochem. Energy Rev.* **2022**, *5*, 1. [CrossRef]
4. Yan, Y.; Wang, P.; Lin, J.; Cao, J.; Qi, J. Modification strategies on transition metal-based electrocatalysts for efficient water splitting. *J. Energy Chem.* **2021**, *58*, 446–462. [CrossRef]
5. Cao, X.; Wang, T.; Jiao, L. Transition-metal (Fe, Co, and Ni)-based nanofiber electrocatalysts for water splitting. *Adv. Fiber Mater.* **2021**, *3*, 210–228. [CrossRef]
6. Guo, Y.; Park, T.; Yi, J.W.; Henzie, J.; Kim, J.; Wang, Z.; Jiang, B.; Bando, Y.; Sugahara, Y.; Tang, J.; et al. Nanoarchitectonics for transition-metal-sulfide-based electrocatalysts for water splitting. *Adv. Mater.* **2019**, *31*, 1807134. [CrossRef]
7. Yu, Y.; Zhou, J.; Sun, Z. Novel 2D Transition-Metal Carbides: Ultrahigh Performance Electrocatalysts for Overall Water Splitting and Oxygen Reduction. *Adv. Funct. Mater.* **2020**, *30*, 2000570. [CrossRef]
8. Su, H.; Jiang, J.; Song, S.; An, B.; Li, N.; Gao, Y.; Ge, L. Recent progress on design and applications of transition metal chalcogenide-associated electrocatalysts for the overall water splitting. *Chin. J. Catal.* **2023**, *44*, 7–49. [CrossRef]
9. Peng, X.; Yan, Y.; Jin, X.; Huang, C.; Jin, W.; Gao, B.; Chu, P.K. Recent advance and prospectives of electrocatalysts based on transition metal selenides for efficient water splitting. *Nano Energy* **2020**, *78*, 105234. [CrossRef]
10. Ali, A.; Shen, P.K. Nonprecious metal's graphene-supported electrocatalysts for hydrogen evolution reaction: Fundamentals to applications. *Carbon Energy* **2020**, *2*, 99–121. [CrossRef]
11. Sun, H.; Xu, X.; Kim, H.; Jung, W.; Zhou, W.; Shao, Z. Electrochemical water splitting: Bridging the gaps between fundamental research and industrial applications. *Energy Environ. Mater.* **2022**, *2022*, e12441. [CrossRef]
12. Fu, H.C.; Varadhan, P.; Tsai, M.L.; Li, W.; Ding, Q.; Lin, C.H.; Bonifazi, M.; Fratalocchi, A.; Jin, S.; He, J.H. Improved performance and stability of photoelectrochemical water-splitting Si system using a bifacial design to decouple light harvesting and electrocatalysis. *Nano Energy* **2020**, *70*, 104478. [CrossRef]
13. Kumar, M.; Meena, B.; Subramanyam, P.; Suryakala, D.; Subrahmanyam, C. Recent trends in photoelectrochemical water splitting: The role of cocatalysts. *NPG Asia Mater.* **2022**, *14*, 88. [CrossRef]
14. Wang, S.; Yang, P.; Sun, X.; Xing, H.; Hu, J.; Chen, P.; Cui, Z.; Zhu, W.; Ma, Z. Synthesis of 3D heterostructure Co-doped Fe_2P electrocatalyst for overall seawater electrolysis. *Appl. Catal. B Environ.* **2021**, *297*, 120386. [CrossRef]
15. Zhao, Y.; You, J.; Wang, L.; Bao, W.; Yao, R. Recent advances in Ni_3S_2-based electrocatalysts for oxygen evolution reaction. *Int. J. Hydrogen Energy* **2021**, *46*, 39146–39182. [CrossRef]
16. Li, Y.; Sun, Y.; Qin, Y.; Zhang, W.; Wang, L.; Luo, M.; Yang, H.; Guo, S. Recent advances on water-splitting electrocatalysis mediated by noble-metal-based nanostructured materials. *Adv. Energy Mater.* **2020**, *10*, 1903120. [CrossRef]
17. Xu, H.; Zhao, Y.; He, G.; Chen, H. Race on engineering noble metal single-atom electrocatalysts for water splitting. *Int. J. Hydrogen Energy* **2022**, *47*, 14257–14279. [CrossRef]
18. Zhang, J.; Lian, J.; Jiang, Q.; Wang, G. Boosting the OER/ORR/HER activity of Ru-doped Ni/Co oxides heterostructure. *Chem. Eng. J.* **2022**, *439*, 135634. [CrossRef]
19. Lin, S.; Yu, Y.; Sun, D.; Meng, F.; Chu, W.; Huang, L.; Ren, J.; Su, Q.; Ma, S.; Xu, B. $FeNi_2P$ three-dimensional oriented nanosheet array bifunctional catalysts with better full water splitting performance than the full noble metal catalysts. *J. Colloid Interface Sci.* **2022**, *608*, 2192–2202. [CrossRef]
20. Sun, H.; Xu, X.; Song, Y.; Zhou, W.; Shao, Z. Designing high-valence metal sites for electrochemical water splitting. *Adv. Funct. Mater.* **2021**, *31*, 2009779. [CrossRef]
21. Chatenet, M.; Pollet, B.G.; Dekel, D.R.; Dionigi, F.; Deseure, J.; Millet, P.; Braatz, R.D.; Bazant, M.Z.; Eikerling, M.; Staffell, I.; et al. Water electrolysis: From textbook knowledge to the latest scientific strategies and industrial developments. *Chem. Soc. Rev.* **2022**, *51*, 4583–4762. [CrossRef] [PubMed]
22. Luo, W.; Wang, Y.; Cheng, C. Ru-based electrocatalysts for hydrogen evolution reaction: Recent research advances and perspectives. *Mater. Today Phys.* **2020**, *15*, 100274. [CrossRef]
23. Gong, Y.; Yao, J.; Wang, P.; Li, Z.; Zhou, H.; Xu, C. Perspective of hydrogen energy and recent progress in electrocatalytic water splitting. *Chin. J. Chem. Eng.* **2022**, *43*, 282–296. [CrossRef]
24. Darband, G.B.; Aliofkhazraei, M.; Rouhaghdam, A.S.; Kiani, M.A. Three-dimensional Ni-Co alloy hierarchical nanostructure as efficient non-noble-metal electrocatalyst for hydrogen evolution reaction. *Appl. Surf. Sci.* **2019**, *465*, 846–862. [CrossRef]
25. Darband, G.B.; Aliofkhazraei, M.; Rouhaghdam, A.S. Facile electrodeposition of ternary Ni-Fe-Co alloy nanostructure as a binder free, cost-effective and durable electrocatalyst for high-performance overall water splitting. *J. Colloid Interface Sci.* **2019**, *547*, 407–420. [CrossRef]
26. Nie, M.; Sun, H.; Gao, Z.D.; Li, Q.; Xue, Z.H.; Luo, J.; Liao, J.M. Co–Ni nanowires supported on porous alumina as an electrocatalyst for the hydrogen evolution reaction. *Electrochem. Commun.* **2020**, *115*, 106719. [CrossRef]

27. Xu, Y.; Dong, X.; Miao, J.; Wang, S.; Liu, Z.; Zhai, Z.; Zhang, L.; Liu, Z. Facile preparation of Ni, Co-alloys supported on porous carbon spheres for supercapacitors and hydrogen evolution reaction application. *Int. J. Hydrogen Energy* **2020**, *45*, 1466–1476. [CrossRef]
28. Ashraf, M.A.; Li, C.; Pham, B.T.; Zhang, D. Electrodeposition of Ni–Fe–Mn ternary nanosheets as affordable and efficient electrocatalyst for both hydrogen and oxygen evolution reactions. *Int. J. Hydrogen Energy* **2020**, *45*, 24670–24683. [CrossRef]
29. Zhou, J.; Xiao, H.; Weng, W.; Gu, D.; Xiao, W. Interfacial confinement of Ni-V_2O_3 in molten salts for enhanced electrocatalytic hydrogen evolution. *J. Energy Chem.* **2020**, *50*, 280–285. [CrossRef]
30. Browne, M.P.; Sofer, Z.; Pumera, M. Layered and two dimensional metal oxides for electrochemical energy conversion. *Energy Environ. Sci.* **2019**, *12*, 41–58. [CrossRef]
31. Li, C.; Zhang, B.; Li, Y.; Hao, S.; Cao, X.; Yang, G.; Wu, J.; Huang, Y. Self-assembled Cu-Ni bimetal oxide 3D in-plane epitaxial structures for highly efficient oxygen evolution reaction. *Appl. Catal. B Environ.* **2019**, *244*, 56–62. [CrossRef]
32. Yu, M.; Budiyanto, E.; Tüysüz, H. Principles of water electrolysis and recent progress in cobalt-, nickel-, and iron-based oxides for the oxygen evolution reaction. *Angew. Chem. Int. Ed.* **2022**, *61*, e202103824.
33. Ma, X.; Wei, P.; Yang, Y.; Kang, H.; Guo, D.; Liu, L. One-pot synthesis of Ni-Co layered double hydroxide nanosheets as efficient catalysts for oxygen evolution reaction. *Mater. Today Commun.* **2019**, *20*, 100596. [CrossRef]
34. Gao, G.; Wang, K.; Wang, X. Peony flower-like Cu_xS@NiMn LDH heterostructure as an efficient electrocatalyst for the oxygen evolution reaction. *Int. J. Hydrogen Energy* **2023**, *48*, 1347–1359. [CrossRef]
35. Li, H.; Wang, X.; Wang, T.; Xiao, F. A facile, green and time-saving method to prepare partially crystalline NiFe layered double hydroxide nanosheets on nickel foam for superior OER catalysis. *J. Alloys Compd.* **2020**, *844*, 156224. [CrossRef]
36. Zhu, W.; Chen, W.; Yu, H.; Zeng, Y.; Ming, F.; Liang, H.; Wang, Z. NiCo/NiCo–OH and NiFe/NiFe–OH core shell nanostructures for water splitting electrocatalysis at large currents. *Appl. Catal. B Environ.* **2020**, *278*, 119326. [CrossRef]
37. Li, L.F.; Li, Y.F.; Liu, Z.P. Oxygen evolution activity on NiOOH catalysts: Four-coordinated Ni cation as the active site and the hydroperoxide mechanism. *ACS Catal.* **2020**, *10*, 2581–2590. [CrossRef]
38. Ullah, H.; Loh, A.; Trudgeon, D.P.; Li, X. Density functional theory study of NiFeCo trinary oxy-hydroxides for an efficient and stable oxygen evolution reaction catalyst. *ACS Omega* **2020**, *5*, 20517–20524. [CrossRef]
39. Vandichel, M.; Laasonen, K.; Kondov, I. Oxygen evolution and reduction on Fe-doped NiOOH: Influence of solvent, dopant position and reaction mechanism. *Top. Catal.* **2020**, *63*, 833–845. [CrossRef]
40. Pi, C.; Huang, C.; Yang, Y.; Song, H.; Zhang, X.; Zheng, Y.; Gao, B.; Fu, J.; Chu, P.K.; Huo, K. In situ formation of N-doped carbon-coated porous MoP nanowires: A highly efficient electrocatalyst for hydrogen evolution reaction in a wide pH range. *Appl. Catal. B Environ.* **2020**, *263*, 118358. [CrossRef]
41. Yan, Q.; Chen, X.; Wei, T.; Wang, G.; Zhu, M.; Zhuo, Y.; Cheng, K.; Ye, K.; Zhu, K.; Yan, J.; et al. Hierarchical edge-rich nickel phosphide nanosheet arrays as efficient electrocatalysts toward hydrogen evolution in both alkaline and acidic conditions. *ACS Sustain. Chem. Eng.* **2019**, *7*, 7804–7811. [CrossRef]
42. Ma, B.; Yang, Z.; Chen, Y.; Yuan, Z. Nickel cobalt phosphide with three-dimensional nanostructure as a highly efficient electrocatalyst for hydrogen evolution reaction in both acidic and alkaline electrolytes. *Nano Res.* **2019**, *12*, 375–380. [CrossRef]
43. Ge, R.; Huo, J.; Liao, T.; Liu, Y.; Zhu, M.; Li, Y.; Zhang, J.; Li, W. Hierarchical molybdenum phosphide coupled with carbon as a whole pH-range electrocatalyst for hydrogen evolution reaction. *Appl. Catal. B Environ.* **2020**, *260*, 118196. [CrossRef]
44. Zhou, M.; Sun, Q.; Shen, Y.; Ma, Y.; Wang, Z.; Zhao, C. Fabrication of 3D microporous amorphous metallic phosphides for high-efficiency hydrogen evolution reaction. *Electrochim. Acta* **2019**, *306*, 651–659. [CrossRef]
45. Zhu, L.; Liu, L.; Huang, G.; Zhao, Q. Hydrogen evolution over N-doped CoS_2 nanosheets enhanced by superaerophobicity and electronic modulation. *Appl. Surf. Sci.* **2020**, *504*, 144490. [CrossRef]
46. Guo, X.; Liu, Z.; Liu, F.; Zhang, J.; Zheng, L.; Hu, Y.; Mao, J.; Liu, H.; Xue, Y.; Tang, C. Sulfur vacancy-tailored $NiCo_2S_4$ nanosheet arrays for the hydrogen evolution reaction at all pH values. *Catal. Sci. Technol.* **2020**, *10*, 1056–1065. [CrossRef]
47. Chen, S.; Liang, W.; Wang, X.; Zhao, Y.; Wang, S.; Li, Z.; Wang, S.; Hou, L.; Jiang, Y.; Gao, F. P-doped MOF-derived CoNi bimetallic sulfide electrocatalyst for highly-efficiency overall water splitting. *J. Alloys Compd.* **2023**, *931*, 167575. [CrossRef]
48. Zahra, R.; Pervaiz, E.; Baig, M.M.; Rabi, O. Three-dimensional hierarchical flowers-like cobalt-nickel sulfide constructed on graphitic carbon nitride: Bifunctional non-noble electrocatalyst for overall water splitting. *Electrochim. Acta* **2022**, *418*, 140346. [CrossRef]
49. Wang, J.; Shao, H.; Ren, S.; Hu, A.; Li, M. Fabrication of porous Ni-Co catalytic electrode with high performance in hydrogen evolution reaction. *Appl. Surf. Sci.* **2021**, *539*, 148045. [CrossRef]
50. Pan, Q.Q.; Xu, C.Y.; Li, X.; Zhang, J.F.; Hu, X.L.; Geng, Y.; Su, Z.M. Porous Ni-Mo bimetallic hybrid electrocatalyst by intermolecular forces in precursors for enhanced hydrogen generation. *Chem. Eng. J.* **2021**, *405*, 126962. [CrossRef]
51. Ros, C.; Murcia-López, S.; Garcia, X.; Rosado, M.; Arbiol, J.; Llorca, J.; Morante, J.R. Facing seawater splitting challenges by regeneration with Ni−Mo−Fe bifunctional electrocatalyst for hydrogen and oxygen evolution. *ChemSusChem* **2021**, *14*, 2872–2881. [CrossRef]
52. Zhang, Z.; Wu, Y.; Zhang, D. Potentiostatic electrodeposition of cost-effective and efficient Ni–Fe electrocatalysts on Ni foam for the alkaline hydrogen evolution reaction. *Int. J. Hydrogen Energy* **2022**, *47*, 1425–1434. [CrossRef]
53. Sun, J.; Yu, B.; Tan, F.; Yang, W.; Cheng, G.; Zhang, Z. High throughput preparation of Ni–Mo alloy thin films as efficient bifunctional electrocatalysts for water splitting. *Int. J. Hydrogen Energy* **2022**, *47*, 15764–15774. [CrossRef]

54. Badrnezhad, R.; Nasri, F.; Pourfarzad, H.; Jafari, S.K. Effect of iron on Ni–Mo–Fe composite as a low-cost bifunctional electrocatalyst for overall water splitting. *Int. J. Hydrogen Energy* **2021**, *46*, 3821–3832. [CrossRef]
55. Niu, J.; Yue, Y.; Yang, C.; Wang, Y.; Qin, J.; Zhang, X.; Wu, Z.S. Ultrarapid synthesis Ni-Cu bifunctional electrocatalyst by self-etching electrodeposition for high-performance water splitting reaction. *Appl. Surf. Sci.* **2021**, *561*, 150030. [CrossRef]
56. Gao, W.; Zou, Y.; Zang, Y.; Zhao, X.; Zhou, W.; Dai, Y.; Liu, H.; Wang, J.J.; Ma, Y.; Sang, Y. Magnetic-field-regulated Ni-Fe-Mo ternary alloy electrocatalysts with enduring spin polarization enhanced oxygen evolution reaction. *Chem. Eng. J.* **2023**, *455*, 140821. [CrossRef]
57. Yuan, H.; Zheng, S.; Sang, S.; Yang, J.; Sun, J.; Ma, Z.; Wang, X. Three-dimensional hierarchical nanoporous (Mn, Ni)-Doped Cu_2S architecture towards high-efficiency overall water splitting. *Int. J. Hydrogen Energy* **2022**, *47*, 11827–11840. [CrossRef]
58. Luo, J.; Guo, W.H.; Zhang, Q.; Wang, X.H.; Shen, L.; Fu, H.C.; Wu, L.L.; Chen, X.H.; Luo, H.Q.; Li, N.B. One-pot synthesis of Mn–Fe bimetallic oxide heterostructures as bifunctional electrodes for efficient overall water splitting. *Nanoscale* **2020**, *12*, 19992–20001. [CrossRef]
59. Xu, P.; Qiu, L.; Wei, L.; Liu, Y.; Yuan, D.; Wang, Y.; Tsiakaras, P. Efficient overall water splitting over Mn doped Ni_2P microflowers grown on nickel foam. *Catal. Today* **2020**, *355*, 815–821. [CrossRef]
60. Li, Y.; Dong, Z.; Jiao, L. Multifunctional transition metal-based phosphides in energy-related electrocatalysis. *Adv. Energy Mater.* **2020**, *10*, 1902104. [CrossRef]
61. Gbadamasi, S.; Mohiuddin, M.; Krishnamurthi, V.; Verma, R.; Khan, M.W.; Pathak, S.; Kalantar-Zadeh, K.; Mahmood, N. Interface chemistry of two-dimensional heterostructures–fundamentals to applications. *Chem. Soc. Rev.* **2021**, *50*, 4684–4729. [CrossRef] [PubMed]
62. Xu, X.; Tian, X.; Zhong, Z.; Kang, L.; Yao, J. In-situ growth of iron/nickel phosphides hybrid on nickel foam as bifunctional electrocatalyst for overall water splitting. *J. Power Sources* **2019**, *424*, 42–51. [CrossRef]
63. Sahoo, D.P.; Das, K.K.; Mansingh, S.; Sultana, S.; Parida, K. Recent progress in first row transition metal Layered double hydroxide (LDH) based electrocatalysts towards water splitting: A review with insights on synthesis. *Coord. Chem. Rev.* **2022**, *469*, 214666. [CrossRef]
64. Sumboja, A.; Chen, J.; Zong, Y.; Lee, P.S.; Liu, Z. NiMn layered double hydroxides as efficient electrocatalysts for the oxygen evolution reaction and their application in rechargeable Zn–air batteries. *Nanoscale* **2017**, *9*, 774–780. [CrossRef]
65. Wang, P.; Qi, J.; Li, C.; Li, W.; Wang, T.; Liang, C. Hierarchical $CoNi_2S_4$@NiMn-layered double hydroxide heterostructurenanoarrays on superhydrophilic carbon cloth for enhanced overall water splitting. *Electrochim. Acta* **2020**, *345*, 136247. [CrossRef]
66. Wang, P.; Qi, J.; Chen, X.; Li, C.; Li, W.; Wang, T.; Liang, C. Three-dimensional heterostructured NiCoP@NiMn-layered double hydroxide arrays supported on Ni foam as a bifunctional electrocatalyst for overall water splitting. *ACS Appl. Mater. Interfaces* **2019**, *12*, 4385–4395. [CrossRef]
67. Yang, L.; Chen, L.; Yang, D.; Yu, X.; Xue, H.; Feng, L. NiMn layered double hydroxide nanosheets/$NiCo_2O_4$ nanowires with surface rich high valence state metal oxide as an efficient electrocatalyst for oxygen evolution reaction. *J. Power Sources* **2018**, *392*, 23–32. [CrossRef]
68. Wang, Y.; Liu, X.; Zhang, N.; Qiu, G.; Ma, R. Cobalt-doped Ni–Mn layered double hydroxide nanoplates as high-performance electrocatalyst for oxygen evolution reaction. *Appl. Clay Sci.* **2018**, *165*, 277–283. [CrossRef]
69. Khan, R.; Mehran, M.T.; Baig, M.M.; Sarfraz, B.; Naqvi, S.R.; Niazi, M.B.K.; Khan, M.Z.; Khoja, A.H. 3D hierarchical Heterostructured LSTN@NiMn-layered double hydroxide as a bifunctional water splitting electrocatalyst for hydrogen production. *Fuel* **2021**, *285*, 119174. [CrossRef]
70. Jiang, D.; Ma, W.; Yang, R.; Quan, B.; Li, D.; Meng, S.; Chen, M. Nickel–manganese bimetallic phosphides porous nanosheet arrays as highly active bifunctional hydrogen and oxygen evolution electrocatalysts for overall water splitting. *Electrochim. Acta* **2020**, *329*, 135121. [CrossRef]
71. Zhang, G.; Ge, H.; Zhao, L.; Liu, J.; Wang, F.; Fan, S.; Li, G. $NiMn_{1.5}PO_4$ thin layer supported on Ni foam as a highly efficient bifunctional electrocatalyst for overall water splitting. *Electrochim. Acta* **2021**, *367*, 137567. [CrossRef]
72. Maleki, M.; Darband, G.B.; Rouhaghdam, A.S.; Andaveh, R.; Kazemi, Z.M. Mn-incorporated nickel selenide: An ultra-active bifunctional electrocatalyst for hydrogen evolution and urea oxidation reactions. *Chem. Commun.* **2022**, *58*, 3545–3548. [CrossRef] [PubMed]
73. Taherinia, D.; Hatami, H.; Valadi, F.M. Trimetallic Co-Ni-Mn metal-organic framework as an efficient electrocatalyst for alkaline oxygen evolution reaction. *J. Electroanal. Chem.* **2022**, *922*, 116720. [CrossRef]
74. Luo, L.; Huang, H.; Yang, Y.; Gong, S.; Li, Y.; Wang, Y.; Luo, W.; Li, Z. Nickel and manganese oxide heterostructure nanoparticles supported by carbon nanotube for highly efficient oxygen evolution reaction catalysis. *Appl. Surf. Sci.* **2022**, *575*, 151699. [CrossRef]
75. Luo, Y.; Wang, P.; Zhang, G.; Wu, S.; Chen, Z.; Ranganathan, H.; Sun, S.; Shi, Z. Mn-doped nickel–iron phosphide heterointerface nanoflowers for efficient alkaline freshwater/seawater splitting at high current densities. *Chem. Eng. J.* **2023**, *454*, 140061. [CrossRef]
76. Huang, H.; Hu, X.; Hou, Z.; Yang, D.; Xiang, D.; Hu, L. Interfacial construction and lattice distortion-triggered bifunctionality of Mn-NiS/Mn-Ni_3S_4 for H_2 production. *Fuel* **2022**, *328*, 125337. [CrossRef]
77. Hatami, E.; Toghraei, A.; Darband, G.B. Electrodeposition of Ni–Fe micro/nano urchin-like structure as an efficient electrocatalyst for overall water splitting. *Int. J. Hydrogen Energy* **2021**, *46*, 9394–9405. [CrossRef]

78. Kim, C.; Lee, S.; Kim, S.H.; Park, J.; Kim, S.; Kwon, S.H.; Bae, J.S.; Park, Y.S.; Kim, Y. Cobalt–iron–phosphate hydrogen evolution reaction electrocatalyst for solar-driven alkaline seawater electrolyzer. *Nanomataterials* **2021**, *11*, 2989. [CrossRef]
79. Sun, Y.Y.; Jiang, M.Y.; Wu, L.K.; Hou, G.Y.; Tang, Y.P.; Liu, M. Ultra-thin NiFeSe nanosheets as a highly efficient bifunctional electrocatalyst for overall water splitting. *Sustain. Energy Fuels* **2020**, *4*, 582–588. [CrossRef]
80. Zhu, M.; Bai, X.; Yan, Q.; Yan, Y.; Zhu, K.; Ye, K.; Yan, J.; Cao, D.; Huang, X.; Wang, G. Iron molybdenum selenide supported on reduced graphene oxide as an efficient hydrogen electrocatalyst in acidic and alkaline media. *J. Colloid Interface Sci.* **2021**, *602*, 384–393. [CrossRef]
81. Laszczyńska, A.; Tylus, W.; Szczygieł, I. Electrocatalytic properties for the hydrogen evolution of the electrodeposited Ni–Mo/WC composites. *Int. J. Hydrogen Energy* **2021**, *46*, 22813–22831. [CrossRef]
82. Dai, Z.; Du, X.; Zhang, X. The synthesis of Ni-Co-Fe-Se@NiCo-LDH nanoarrays on Ni foam as efficient overall water splitting electrocatalyst. *J. Alloys Compd.* **2023**, *946*, 169451. [CrossRef]
83. Van Phuc, T.; Jana, J.; Ravi, N.; Kang, S.G.; Chung, J.S.; Choi, W.M.; Hur, S.H. Highly active Ni/Co-metal organic framework bifunctional electrocatalyst for water splitting reaction. *Int. J. Hydrogen Energy* **2022**, *47*, 22787–22795. [CrossRef]
84. Bao, F.; Kemppainen, E.; Dorbandt, I.; Bors, R.; Xi, F.; Schlatmann, R.; van de Krol, R.; Calnan, S. Understanding the Hydrogen Evolution Reaction Kinetics of Electrodeposited Nickel-Molybdenum in Acidic, Near-Neutral, and Alkaline Conditions. *ChemElectroChem* **2021**, *8*, 195–208. [CrossRef]
85. Hussain, S.; Rabani, I.; Vikraman, D.; Feroze, A.; Karuppasamy, K.; Haq, Z.U.; Seo, Y.S.; Chun, S.H.; Kim, H.S.; Jung, J. Hybrid design using carbon nanotubes decorated with Mo_2C and W_2C nanoparticles for supercapacitors and hydrogen evolution reactions. *ACS Sustain. Chem. Eng.* **2020**, *8*, 12248–12259. [CrossRef]
86. Yang, C.; Zhao, R.; Xiang, H.; Wu, J.; Zhong, W.; Li, W.; Zhang, Q.; Yang, N.; Li, X. Ni-activated transition metal carbides for efficient hydrogen evolution in acidic and alkaline solutions. *Adv. Energy Mater.* **2020**, *10*, 2002260. [CrossRef]
87. Caliskan, S.; Wang, A.; Qin, F.; House, S.D.; Lee, J.K. Molybdenum Carbide-Reduced Graphene Oxide Composites as Electrocatalysts for Hydrogen Evolution. *ACS Appl. Nano Mater.* **2022**, *5*, 3790–3798. [CrossRef]
88. Sun, Y.; Peng, F.; Zhang, L.; Jiang, B.; Dou, H.; Zhang, N.; Xu, M.; Yang, N. Hierarchical Nitrogen-doped Mo_2C Nanoparticle-in-microflower Electrocatalyst: In Situ Synthesis and Efficient Hydrogen-evolving Performance in Alkaline and Acidic Media. *ChemCatChem* **2020**, *12*, 6040–6049. [CrossRef]
89. Eiler, K.; Suriñach, S.; Sort, J.; Pellicer, E. Mesoporous Ni-rich Ni–Pt thin films: Electrodeposition, characterization and performance toward hydrogen evolution reaction in acidic media. *Appl. Catal. B Environ.* **2020**, *265*, 118597. [CrossRef]
90. El-Refaei, S.M.; Russo, P.A.; Schultz, T.; Koch, N.; Pinna, N. Dual doping of MoP with M (Mn, Fe) and S to achieve high hydrogen evolution reaction activity in both acidic and alkaline media. *ChemCatChem* **2021**, *13*, 4392–4402. [CrossRef]
91. Song, H.; Guo, S.; Zhang, X.; Yang, Y.; Gao, B.; Pi, Y.; Pi, C.; Chu, P.K.; Huo, K. In-Situ and controllable construction of Mo_2N embedded Mo_2C nanobelts as robust electrocatalyst for superior pH-universal hydrogen evolution reaction. *J. Alloys Compd.* **2022**, *918*, 165611. [CrossRef]
92. Chen, T.; Qian, M.; Tong, X.; Liao, W.; Fu, Y.; Dai, H.; Yang, Q. Nanosheet self-assembled NiCoP microflowers as efficient bifunctional catalysts (HER and OER) in alkaline medium. *Int. J. Hydrogen Energy* **2021**, *46*, 29889–29895. [CrossRef]
93. Bhat, K.S.; Nagaraja, H.S. In situ synthesis of copper sulfide-nickel sulfide arrays on three-dimensional nickel foam for overall water splitting. *ChemistrySelect* **2020**, *5*, 2455–2464. [CrossRef]
94. Li, Z.; Wang, X.; Wang, X.; Lin, Y.; Meng, A.; Yang, L.; Li, Q. Mn-Cd-S@amorphous-Ni_3S_2 hybrid catalyst with enhanced photocatalytic property for hydrogen production and electrocatalytic OER. *Appl. Surf. Sci.* **2019**, *491*, 799–806. [CrossRef]
95. Li, B.; Li, Z.; He, F.; Pang, Q.; Shen, P. One-pot preparation of Ni_3S_2@3-D graphene free-standing electrode by simple Q-CVD method for efficient oxygen evolution reaction. *Int. J. Hydrogen Energy* **2019**, *44*, 30806–30819. [CrossRef]